Ionospheric Raytracing in a Time-dependent Mesoscale Ionospheric Model

Katherine A. Zawdie[1], Douglas P. Drob[1] and Joseph D. Huba[2]

[1]Space Science Division, Naval Research Laboratory
4555 Overlook Ave., SW,
Washington, DC 20375

[1]Plasma Physics Division, Naval Research Laboratory
4555 Overlook Ave., SW,
Washington, DC 20375

Abstract

To understand HF radio wave propagation through the ionosphere we have created a new full-physics, ionospheric raytracing model called MOJO (MOdified JOnes-Stephenson). This new code represents a significant advance, capitalizing on modern computational techniques as well as incorporating new understanding of the spatiotemporal variability of the background ionosphere. In this paper we exploit the high-fidelity capabilities of SAMI3 (Sami3 is Another Model of the Ionosphere) and MOJO to simulate traveling ionospheric disturbances (TIDs), examining the relationship between various HF propagation observables and TID characteristics.

1. Introduction

One of the challenges for operators of OTHRs (Over The Horizon Radars) is understanding the received signal output in the presence of multipath and range dependent environments. For typical quiescent ionospheric conditions, the received signal is relatively straightforward to interpret. More complicated ionospheric conditions with tilts and other irregularities, such as from Traveling Ionospheric Disturbances (TIDs), present significant challenges for data interpretation. Many studies have been performed over the past 50 years using HF raytracing codes to explain features of HF propagation observations through perturbed ionospheres.

A particularly relevant example is a recent paper by *Cervera and Harris* [2014], where they examined the impact of a TID on Quasi Vertical Ionograms (QVIs). As explained in the paper, many studies have been done in the past, but their study was the first to use a fully 3D ionospheric ray trace code that also included the effects from the magnetic field. As a first approximation, one can assume that radio waves do not deviate from the initial plane in which they were launched; in this case, only a two dimensional ray trace code is required. Importantly *Cervera and Harris* [2014] demonstrated that a three dimensional ray trace model is necessary in order to model the disturbance features in QVIs.

A limitation of the *Cervera and Harris* [2014] study is that their simulated TID did not vary as a function of cross-range, i.e. the ionospheric gradients were only applied in the along track direction. In this study we use a full-physics ionospheric model to generate a time-dependent, three dimensional ionosphere that includes a synthetic Medium Scale TID (MSTID). The simulated ionosphere includes gradients in all three dimensions. We make use

of a highly modified version of the original Jones-Stephenson [*Jones and Stephenson*, 1975] raytrace algorithm called MOJO (MOdified JOnes code); to examine the effects of MSTIDs on the propagation of radio waves in the ionosphere. We have found that in many cases the radio wave path is not confined to a two dimensional plane and that horizontal gradients in the cross-range direction have a profound impact on the path geometry of radio waves through the ionosphere, and thus the group-delays.

2. Models

The background ionospheres used in this study are generated using SAMI3/ESF [*Huba et al.*, 2008], which is a three-dimensional, physics based model of the ionosphere derived from the two-dimensional model SAMI2 [*Huba et al.*, 2000]. The plasma and chemical evolution of seven ion species (H^+, He^+, O^+, $O2^+$, N^+, N_2^+, and NO^+) are modeled. The code includes 21 chemical reactions plus radiative recombination and simulates plasma along the entire dipole magnetic field line. The electron and ion temperature equations (for three ion species: H^+, He^+ and O^+) are solved. Quasi-neutrality is assumed, so the electron density is determined by summing the densities of each ion species. The neutral composition and temperature are specified using the empirical NRLMSISE00 model [*Picone et al.*, 2002] and the neutral wind is set to a constant for the purposes of this study. The grid is a nonorthogonal, nonuniform fixed grid that is periodic in longitude and simulates a 4° longitudinal wedge of the ionosphere. The magnetic field is a non-tilted dipole so geographic and magnetic latitude are the same.

For these simulations, an additional traveling-wave electric field is added during the calculation of the $E \times B$ drift. The components of the wave in the vertical (p) and horizontal (h) directions are defined as:

$$(\mathbf{E}_{TID} \times \mathbf{B})_{[p,h]} = -U_{TID} \frac{k_{[k,y]}}{k} sin(k_x x + k_y y - \omega t) \tag{1}$$

Here, x and y are Cartesian coordinates corresponding to the longitudinal and latitudinal directions, respectively. The wave numbers k_x and k_y are defined as $k_x = kcos\theta_{TID}$ and $k_y = ksin\theta_{TID}$, where θ_{TID} is the propagation angle. An angle of 0° implies that propagation is parallel to the equator, so the crests are aligned with the magnetic field, whereas an angle of 90° implies propagation perpendicular to the equator. Following *Krall et al.* [2011], we set the drift amplitude (U_{TID}) to 50 m/s, the wavelength to 250 km, the period to 1 hour and the propagation direction to south-west ward.

As in other SAMI3/ESF studies, the simulation is initialized using output from SAMI2, in this case, for day of year 80 (equinox). The $F_{10.7} = F_{10.7a} = 150$, and the Ap = 4. The longitudinal extent of the simulation is 4°, and it is centered on 0°. The simulations run for one hour, starting at 19:30 local-time (after the lifting of the F layer by the pre-reversal enhancement) and ending at 20:30 LT. Three different simulations are run, which are identical except for the MSTID parameters. The first case, which we refer to as the background case, does not have an MSTID perturbation. The second case has an MSTID imposed with an angle (θ_{TID}) of 20° and the third case has an MSTID with an angle of 50°.

Once the ionospheric electron density fields are generated, MoJo is used to evaluate the HF propagation characteristics within a localized low-latitude region for high vertical incidence propagation. MOJO represents a radical departure from the original Jones-Stephenson

code, as it was updated to take advantage of modern computational techniques and to make it more suitable for use in simulations with a large number of rays. Like the original Jones-Stephenson code, the basic equations take into account the earth's magnetic field so that both O-mode and X-mode rays can be simulated. The ray tracing is three dimensional and takes into account the curvature of the earth. In addition, a number of improvements have been made to the physics equations, such as the inclusion of 3D collision frequencies and deviative absorption.

An important aspect of the raytracing is the ability to compute eigenrays; the specific ray paths that connect a source and receiver. Determination of these paths are required to accurately compute synthetic ionograms and QVIs (c.f. *Cervera and Harris*, [2014]). An iterative shooting method (c.f. *Press et al.*, [1986]) is implemented in MOJO to do this. Numerical approximations of the Jacobian of the target location with respect to launch azimuth and elevation for a given transmission frequency are used to 'home in' on a specific eigenray. Presently an existing eigenray is assumed to be found when the ray misses the receiver by a distance less than δ, where δ is $\sim$O(5 km). For convergence the procedure implemented generally requires an initial reasonable estimate (first guess) in the vicinity of an eigensolution. Unfortunately, situations where multiple eigenrays exist are not handled automatically by the code and must be resolved interactively by refinement of the first guess.

3. Results

Figure 1 shows the electron density as a function of altitude at 10° latitude and 0° longitude at different times for each of the three simulations. The height of the peak density is around 480 km altitude and falls slightly during the hour. The peak density ranges from about 2.9e6/cm^3 to 3.1e6/cm^3, which corresponds to a critical frequency range of about 15-16 MHz. The profiles from the three different simulations are qualitatively very similar. This is because the MSTID primarily creates horizontal gradients rather than simply modifying the electron density profiles. Thus, horizontal gradients are essential for examining the effect on HF propagation.

Figure 2 shows the the (log_{10}) electron density at 290 km altitude as a function of latitude and longitude. The background case (left) has a slight gradient in the latitudinal direction, but it is fairly smooth and much less pronounced than the horizontal gradients introduced by the MSTID simulations. The 20° angle case (center) has gradients in both directions, but the largest horizontal gradients are in the longitudinal direction. In the 50° case (right) the large horizontal gradients are at an angle. Note that in both of the MSTID cases, the minimum/maximum of the density crests are lower/higher than in the background case. In addition, the horizontal gradients are a much smaller scale than the background case.

Next we look at the results from raytracing through the different modeled ionospheres for one time step, in this case at 20:00 LT. Figure 3 shows the ray paths for 3.125 MHz O-mode rays launched from a transmitter located at at 10° latitude, 0° longitude, at an azimuth of 90 ° and varying elevation launch angles that range from 55° to 125°. The left column shows the background case, where the ionosphere does not have large ionospheric gradients. For this case there is no ray bending, and no focusing. The rays all reach their peak heights around 300 km altitude, they are evenly distributed in longitude, and the rays all reach the ground around the 9.5° latitude.

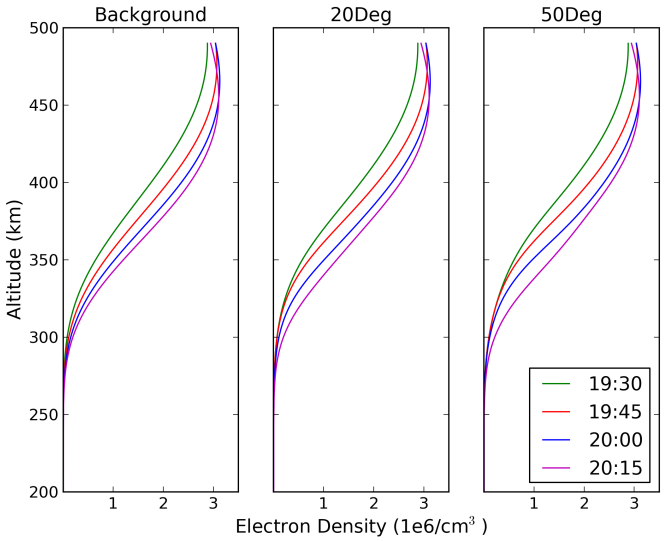

Figure 1: Electron density as a function of altitude at 10° latitude and 0° longitude for 4 different times during each simulation. The left shows the background case (no MSTID). The middle panel shows the case with an imposed MSTID with a 20° propagation angle. The right panel shows the case with an imposed MSTID with a 50° propagation angle.

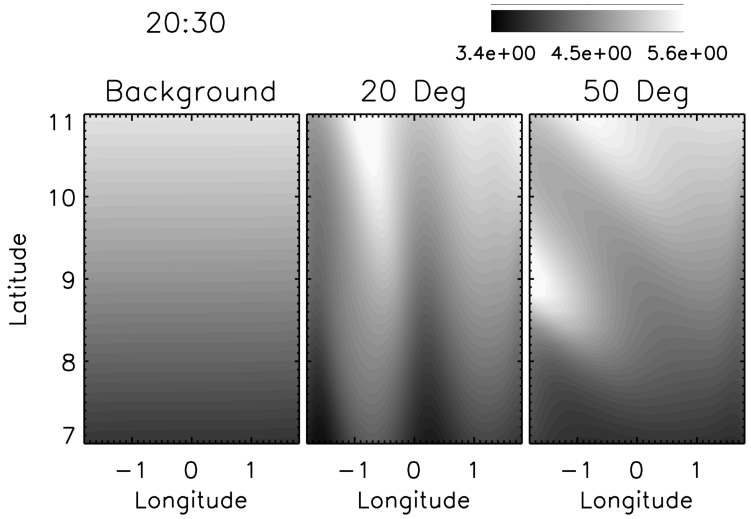

Figure 2: Electron density as a function of latitude and longitude at 290 km altitude. The left shows the background case, the center shows the MSTID with 20° propagation angle, the right shows the MSTID with 50° propagation angle.

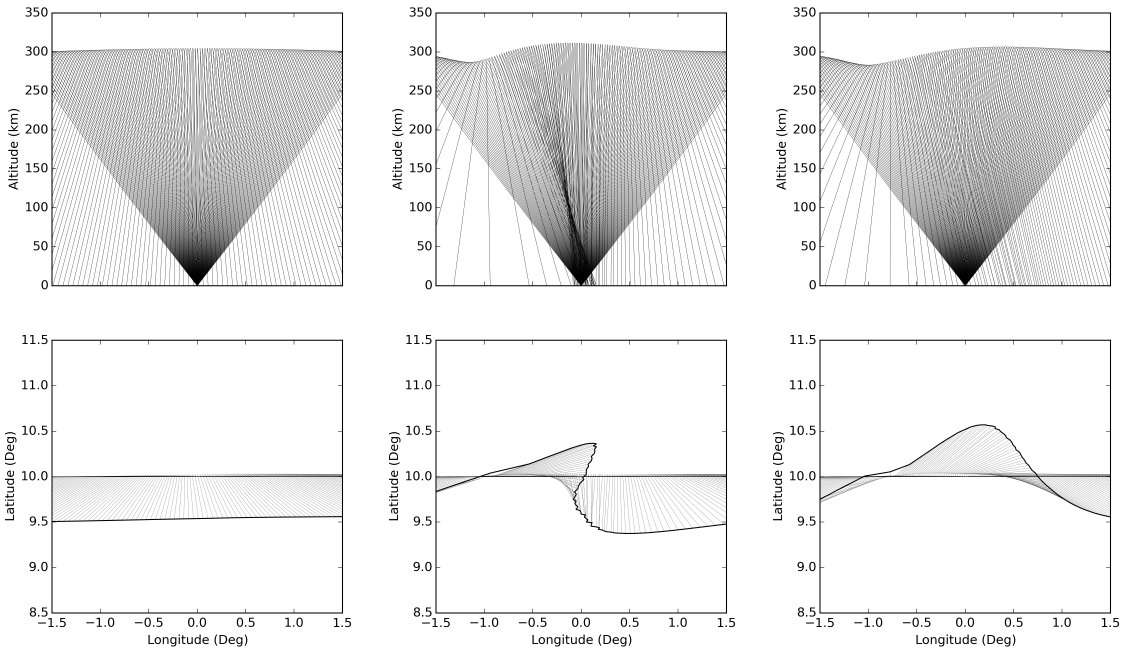

Figure 3: Ray paths from a single transmitter (3.125 MHz O-mode) as a function of longitude-altitude (top row) and longitude- latitude (bottom row) for each of the three simulations. The left column shows the background case, the center shows the case with 20° MSTID, the right shows the case with 50° MSTID.

The center column shows the case 20° MSTID; here the effect of the horizontal gradients are apparent. First, the rays reflect at different altitudes. Next, the top plot seems to show classical focusing around 0° longitude, which we expect for horizontal gradients, but the bottom plot illustrates that this is a mirage. While a large number of rays hit the ground around 0° longitude, they are spread out in latitude, with their final locations ranging from 9.5° to 10.5 degrees, a spread of nearly 100 km.

The right column shows the case with the MSTID propagating at 50°; the effect of horizontal gradients are also noticeable in the ray path here. The rays launched with negative azimuths (towards negative longitude) reflect at a lower altitude than those launched with positive azimuthal angles. There is also focusing towards the positive longitude side. Finally, the rays hit the ground with a one degree latitudinal spread, that ranges from 9.5° to 10.5°.

In both of the MSTID cases the rays deviate significantly from the initial plane, thus two dimensional raytracing would clearly be insufficient to model this phenomenon. In addition, there are significant differences between the 20° and 50° MSTID cases. Thus, cross-range horizontal gradients play a significant role in the ray path.

Figure 4 shows an interesting effect of non-stationary horizontal gradients in the ionosphere. The figure shows how the ray paths change as a function of time between a particular transmitter at 9.1° latitude, 0.1° longitude and a receiver at 10° latitude, 0° longitude. The homing feature was used to find the path for O-mode 3.125 MHz waves for each time step. The blue line shows the path of the ray at 19:30 LT, which reflects at a longitude of about

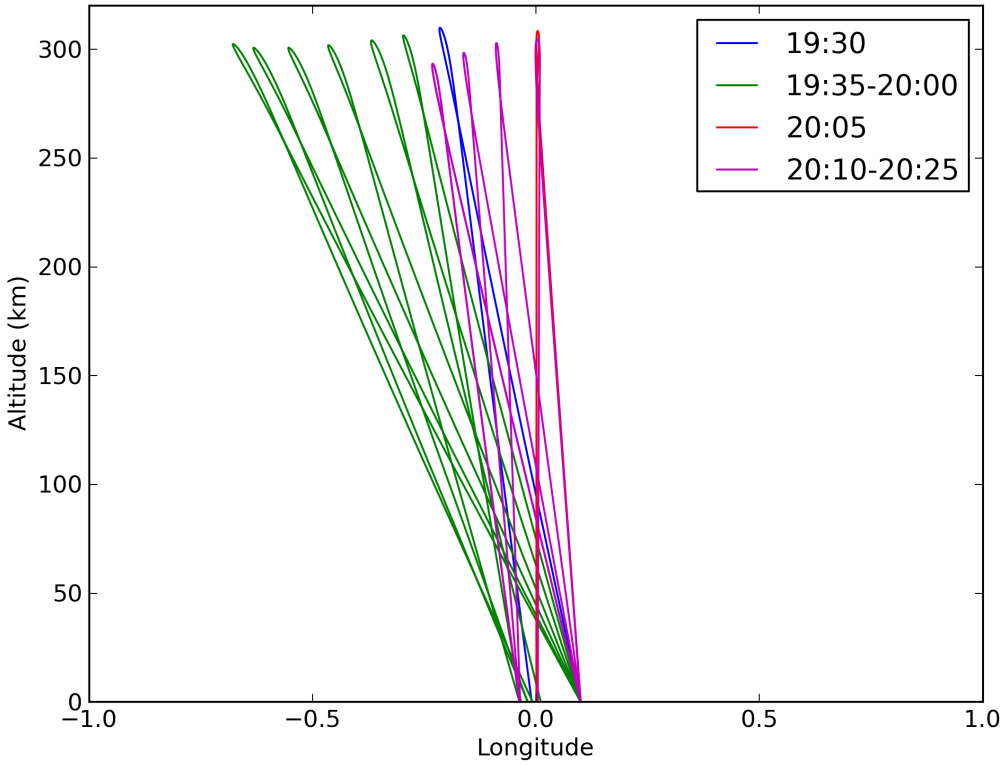

Figure 4: 3.125 MHz O-mode paths between a transmitter at 9.1° latitude, 0.1° longitude and a receiver at 10° latitude and 0° longitude at different times for the for the 20° MSTID case.

-0.1°. The green lines show the ray path for every 5 minutes between 19:35 and 20:00. As time progresses the ray path drifts towards negative longitudes. For example, the ray at 19:45 reflects around -0.4° longitude, but 10 minutes later the ray reflects at -0.6° longitude. At 20:05 (red line), the ray "snaps back" in longitude and reflects at a positive longitude. The magenta shows the continuing progression of the ray after the "snap back". As time continues, the ray drifts towards the negative longitudes again. Note that this is not a small deviation in path, the reflection longitude ranges from 0° to -0.7 ° longitude, which is about 70 km. This ray "snap back" is similar to one that was observed in an HF heating campaign described in *Bernhardt, et al.* [1988].

4. Discussion and Conclusions

For the first time, a realistic full-physics time-dependent mesoscale ionospheric model (SAMI3) of an MSTID has been used for the ionospheric background for HF raytracing. The advantage to this approach is that horizontal gradients in all directions can be taken into account. The result show that these horizontal gradients have a profound effect on the path of the HF rays through the ionosphere. Both three dimensional raytracing and three dimensional

ionospheric gradients are necessary to capture the complexity of radio propagation through the ionosphere.

The addition of an MSTID causes focusing and defocusing, in both the latitudinal and longitudinal directions, with the ray paths dependent on the angle of the MSTID. The addition of an MSTID can cause ray paths to land 100 km away from where they would land with an undisturbed ionosphere. The ray paths between a particular transmitter and receiver can also be affected by the introduction of an MSTID. In this example, the location of reflection varied up to 70 km depending on the simulation time. The change in path length can result in $\sim 3\%$ variation in the group path delay, as well as potentially influence deviative absorption. This also has implications for the simulation of HF heating experiments. Further study is required to examine the effects of these gradients on ionospheric products such as ionograms, QVIs and WSBIs (Wide Sweep Backscatter Ionograms). In addition, MoJo does calculate the doppler shift, which could be compared to observations from various types of ionospheric sounders.

Acknowledgements

K.A. Zawdie and D.P. Drob acknowledge support from the Chief of Naval Research (CNR) as part of the Bottomside Ionosphere (BSI) project under the NRL base program. J.D. Huba acknowledges support from the NRL 6.1 Base Program.

References

Bernhardt, P. A., L. M. Duncan, and C. A. Tepley (1988), Artificial airglow excited by high-power radio waves, *Science 242*, 1022.

Cervera, M. A., and T. J. Harris (2014), Modeling ionospheric disturbance features in quasi-vertically incident ionograms using 3-D magnetoionic ray tracing and atmospheric gravity waves, *J. Geophys. Res. Space Physics, 119*, 431440, doi:10.1002/2013JA019247.

Huba, J. D., G. Joyce, and J. A. Fedder (2000), SAMI2 (Sami2 is another model of the ionosphere): A new low-latitude ionosphere model, *J. Geophys. Res., 105*, 23,03523,053.

Huba, J. D., G. Joyce, and J. Krall (2008), Three dimensional equatorialspread F modeling, *Geophys. Res. Lett., 35*, L10102, doi:10.1029/2008GL033509.

Jones, R. M., and J. J. Stephenson (1975), A versatile three-dimensional ray tracing computer program for radio waves in the ionosphere, *NASA STI/Recon Technical Report N, 76*, 25,476.

Krall, J., J. D. Huba, S. L. Ossakow, G. Joyce, J. J. Makela, E. S. Miller, and M. C. Kelley (2011), Modeling of equatorial plasma bubbles triggered by non equatorial traveling ionospheric disturbances, *Geophys. Res. Lett., 38*, L08103, doi:10.1029/2011GL046890.

Picone, J. M., A. E. Hedin, D. P. Drob, and A. C. Aikin (2002), NRLMSISE-00 empirical model of the atmosphere: Statistical comparisons and scientific issues, *J. Geophys. Res., 107*, 1468, doi:10.1029/2002JA009430.

Press, W. H., Flannery, B. P., Teukolsky, S. A., and Vetterling, W. T. (1986). Numerical recipes: The art of scientific programming. Cambridge UniversityPress, Cambridge, New York.